Integrative and Comparative Biology

Integrative and Comparative Biology, volume 54, number 6, pp. 1014–1025
doi:10.1093/icb/icu100

Society for Integrative and Comparative Biology

SYMPOSIUM

Moving with Bubbles: A Review of the Interactions between Bubbles and the Microorganisms that Surround them

Peter L. L. Walls,* James C. Bird[1,*] and Lydia Bourouiba[1,†]

*Boston University, 730 Commonwealth Avenue, Boston, MA 02215, USA; †Massachusetts Institute of Technology, 77 Massachusetts Avenue, Cambridge, MA 02139, USA

From the symposium "Shaking, Dripping, and Drinking: Surface Tension Phenomena in Organismal Biology" presented at the annual meeting of the Society for Integrative and Comparative Biology, January 3–7, 2014 at Austin, Texas.

[1]E-mail: jbird@bu.edu; lbouro@mit.edu

Synopsis Bubbles are ubiquitous in biological environments, emerging during the complex dynamics of waves breaking in the open oceans or being intentionally formed in bioreactors. From formation, through motion, until death, bubbles play a critical role in the oxygenation and mixing of natural and artificial ecosystems. However, their life is also greatly influenced by the environments in which they emerge. This interaction between bubbles and microorganisms is a subtle affair in which surface tension plays a critical role. Indeed, it shapes the role of bubbles in mixing or oxygenating microorganisms, but also determines how microorganisms affect every stage of the bubble's life. In this review, we guide the reader through the life of a bubble from birth to death, with particular attention to the microorganism–bubble interaction as viewed through the lens of fluid dynamics.

Introduction

The Red tide events associated with algal blooms are among the first examples of phenomena in which bioaerosols were linked to oceanic bursting bubbles. To form the link, Woodcock (1948) sprayed aerosolized seawater containing marine microorganisms into the nose and throat of volunteers, who subsequently developed symptoms of respiratory irritation analogous to those observed in residents of shorelines. Such correlation effectively solidified the earlier hypothesis on the role of bubbles in the creation of marine aerosols (Stuhlman 1932; Jacobs 1937; Woodcock et al. 1953).

In subsequent years, sea spray aerosols have been shown to originate mostly from the bubbles within the foam generated by breaking waves (Boyce 1951; Blanchard 1963) (Fig. 1a). Diseases associated with bursting bubbles are now linked to various pathogen-bearing pools of water such as recreational swimming pools (Falkinham III 2003), hot tubs (Parker et al. 1983; Embil et al. 1997), or wastewater treatment plants (Laitinen et al. 1994; Bauer et al. 2002). Bubbles are, in fact, ubiquitous in biology (Bourouiba and Bush 2012), being responsible for mixing and aeration in the upper layer of the ocean (Blanchard 1989) and for cell mortality in bioreactors from the direct injection of aeration gas (referred to as sparging) (Barbosa et al. 2003; Hu et al. 2011; Murhammer and Goochee 1990; Chisti 2000) and rupture at the surface, for example.

Although bubbles play an important role in a variety of biological systems, our review highlights the physical processes shaping the life of a bubble and its interaction with its biological environment: from its birth in the fluid bulk to its rupture at the fluid surface. We pay particular attention to the contexts of open oceans (Fig. 1A) and closed biological environments (Fig. 1B). In the ocean, the breaking of waves is a ubiquitous process that entrains air and creates bubbles. These bubbles are critical for the healthy functioning and mixing of the ecosystems of the upper surface of the ocean. Similarly, direct and continuous injection of air is vital to the aeration of most bioreactors so as to provide proper oxygenation of their live content (cells or other living forms such as fish). However, the large stresses induced by constant injection of gas can also potentially be detrimental to the health of the cell

Advanced Access publication August 5, 2014

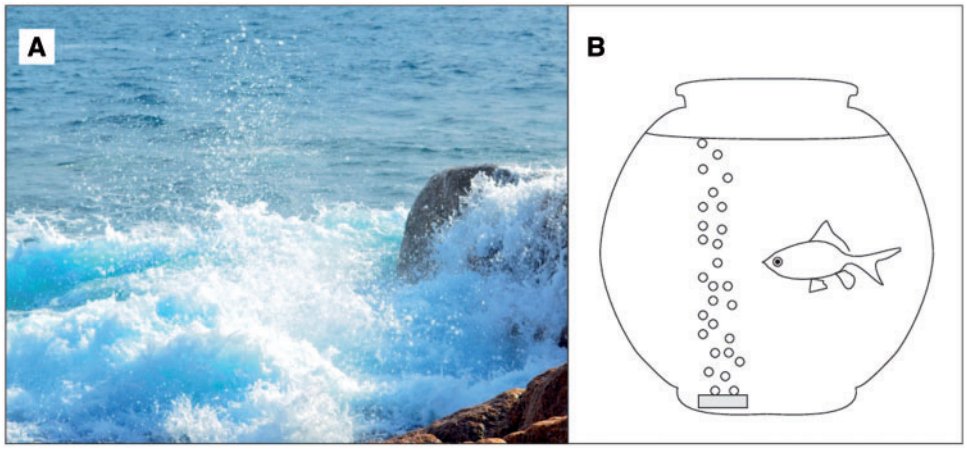

Fig. 1. (A) Wave breaking illustrating the formation of a spectrum of bubbles commonly referred to as white caps. (B) Bubbles may also be deliberately injected into a closed container to aerate the liquid.

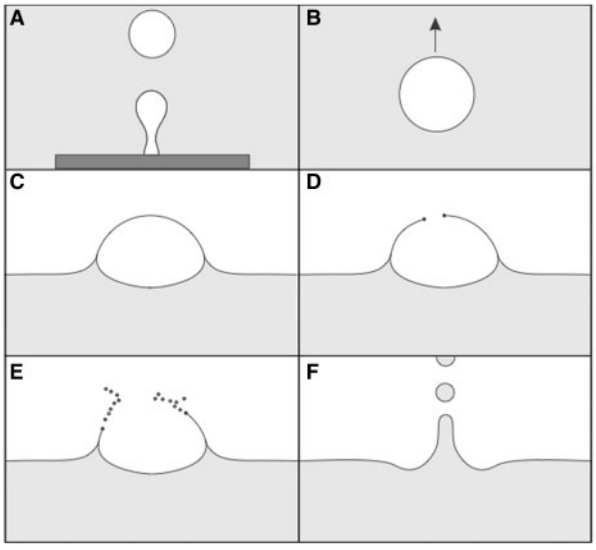

Fig. 2. Various stages in the life of a bubble: (A) formation, (B) rise and dissolution, (C) drainage once at free surface, (D) hole-nucleation and film-retraction, (E) production of film drops, and (F) production of a jet and jet drops.

populations (e.g., Garcia-Briones and Chalmers 1994; Liu et al. 2013)

Once the bubble is formed (Fig. 2A), it begins to rise as a consequence of the gas in the bubble being less dense than the surrounding liquid. While rising, bubbles interact with the surrounding liquid (Bhaga and Weber 1981). The bubble might continue to rise until it reaches the free surface, or alternatively it might completely dissolve into the ambient fluid during its journey. Regardless of its fate, the rising bubble is an efficient biological mixer. Not only is ambient fluid transported in its wake, but also, the bubble can mix the water via the shedding of vortices that can spread laterally (Magnaudet and Eames 2000). Moreover, a bubble can scavenge microorganisms and particles (e.g., viruses, bacteria, cells, and toxins) on its surface, resulting in their passive transport. When reaching the surface (Fig. 2C), the thin film that defines the bubble's boundary drains due to gravitational and capillary forces, until it eventually becomes sufficiently thin for a nucleating hole to grow, the film to retract, and the bubble to pop (Fig. 2D). The retracting film can fragment into numerous film-droplets (Fig. 2E) that can persist well after the bubble is gone. Finally, jet droplets often are created from a jet that forms when the air cavity, that was once the bubble, rapidly equilibrates with its surroundings (Fig. 2F).

Due to the life history of the bubble through the water column, the droplets that it produces can end up being enriched in their content of microorganisms and particles, namely, containing a higher concentration of particulates than that of the bulk fluid that the bubble traversed (Blanchard and Syzdek 1970). In turn, the nature of the particles or organisms, can change the life of a bubble by fundamentally altering its surface and hydrodynamic properties. Not only can biomass influence gas content of a bubble through consumption, but also their size, shape, and surface properties can modify the surface energy and dynamics of the bubble.

We have structured this review by following a bubble's life history from its inception (Fig. 2A and Section "A bubble is born"), throughout its journey through the biological world (Fig. 2B, section 4), to its final destination and rupture (Fig. 2C and D; Section "A bubble drains and dies"); we close by discussing its legacy in the form of residual droplets (Fig. 2E and F; Section "A bubble's legacy lives on").

We aim at presenting these events to an audience that may be less familiar with the concepts of surface tension and fluid mechanics in general and so start by introducing such general concepts in Section "Origin and relevance of capillarity".

Origin and relevance of capillarity

When two fluids are immiscible, such as water and air, the molecules in each fluid are more attracted to like molecules than to the other type. The consequence of this difference in attraction is that work is required to increase the surface area at the interface of the two fluids. The amount of energy ΔE needed to increase the surface area by ΔA is determined by the surface tension γ, such that $\Delta E = \gamma \Delta A$. Therefore, surface tension can be interpreted as energy per unit area, or force per unit length. In this review, forces resulting from surface tension will be referred to as capillary forces, or capillarity.

A spherical bubble with radius R has been schematically split apart in Fig. 3. Surface tension can be interpreted as the amount of tension being applied to the surface; thus, if a force balance were drawn over half of the bubble, the surface tension would manifest itself as a tangential force per unit length acting along the bubble's perimeter (leftward arrows in Fig. 3). If the bubbles were in mechanical equilibrium, the balance of forces implies that there must be a pressure P pushing back against the internal face of the bubble (rightward arrows in Fig. 3). Specifically, the product of the perimeter $2\pi R$ and the average surface tension γ must be equal to the product of the area πR^2 and this pressure P. This force balance leads to $P = 2\gamma/R$, highlighting that the inner pressure of the bubble is higher than that outside by a capillary pressure value P that increases with surface tension and decreases with radius. In other words, for the same surface tension γ a small bubble would have a higher inner pressure than a larger bubble. For the same radius R a bubble made of an interface with a higher surface tension γ would have a higher inner pressure than that with a lower surface-tension interface.

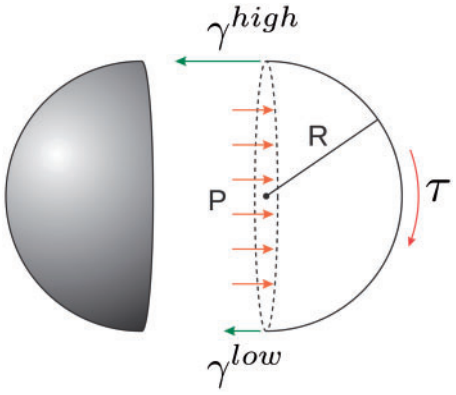

Fig. 3 Illustration of the balance of capillary force and internal pressure force. τ represents the interfacial stress acting on the bubble's surface resulting from the fluid's resistance to the bubble's motion. The imbalance of the surface tensions γ^{high} and γ^{low} will cause a motion of the interface known as Marangoni flow in an attempt to restore balance.

Surface tension can also vary spatially due to thermal or chemical gradients. For example, certain bacteria are known to excrete surfactants that locally reduce surface tension (e.g., Angelini et al. 2009). A gradient of surface tension can thus be generated, resulting in a reactive motion on such an interface. Such motion, referred to as Marangoni flow (Marangoni 1865; Scriven and Sternling 1960) is directed from low γ^{low} to high γ^{high} regions of surface tension; thus redistributing surfactants and effectively opposing the mechanism of generating a gradient of surfactant (Berg et al. 1966; Hosoi and Bush 2001). In Fig. 3 the concentration of surfactants is higher at the bottom of the bubble than at the top. The force balance illustrates that a torque or moment is then generated, resulting in a tangential stress (Clift et al. 1978). At equilibrium, this Marangoni stress is countered by an equal and opposite applied stress τ (as shown Fig. 3).

In general, elements of a bubble are dynamic rather than static. This motion is governed by Newton's second law, which can be re-expressed in the form of the classical Navier–Stokes equation when accounting for the fluid forces involved:

$$\rho\left(\frac{\partial \mathbf{u}}{\partial t} + \mathbf{u}\cdot\nabla\mathbf{u}\right) = -\nabla p + \mu\nabla^2\mathbf{u} + \Delta\rho\mathbf{g}. \quad (1)$$

Here $\mathbf{u}$ is the velocity, t is time, and $\mathbf{g}$ is the gravitational acceleration. Other parameters include ρ and μ, which are the density and dynamic viscosity, respectively, and vary with the phase of the fluid. The difference in the density of gas in the bubble and the density of the surrounding fluid is denoted by $\Delta\rho$.

The left-hand side of Equation (1) is the expanded expression of the mass times acceleration for a unit volume; whereas the right-hand side is the expression of the sum of the forces acting on such unit volume. When physically modeling drops or bubbles, surface tension enters into the pressure term, which is the first term on the right-hand side of Equation (1). Specifically, the surface tension and curvature

directly influence the local pressure, as illustrated in Fig. 3.

For all equations governing physical systems, the dimensions of each term need to be equivalent. It is helpful in both physical and mathematical analysis to non-dimensionalize the equations of motion. This is particularly true in fluid dynamics where the use of dimensionless parameters can also give insight into the physical processes taking place. The relevant dimensionless groups naturally emerge when non-dimensionalizing Equation (1). This process involves first identifying characteristic length-scale L, time-scale or velocity-scale u_c. Each variable is then non-dimensionalized. For example, the dimensional length variable x (or y or z) can be normalized by a characteristic length-scale L, leading to a non-dimensional length variable $\tilde{x} = x/L$. A characteristic length-scale (time, pressure, or velocity, etc.) is that which is relevant to describe the physical dynamics. For example, the characteristic length-scale at which the Earth's rotation becomes important in influencing the atmospheric fluid motion is on the order of 1000 km. Below such characteristic length-scale, the effects of the Earth's rotation are negligible. In particular, this is why, contrary to popular beliefs, the direction of the rotation of water draining from a sink—occurring on a length-scale of centimeters—is not different in the northern and southern hemispheres. It is important to start by identifying the characteristic length and time scales of a problem in fluids. Once identified, non-dimensional variables can be constructed. Here, we follow the convention of denoting non-dimensional variables with a tilde, We can construct a non-dimensional velocity $\tilde{\mathbf{u}} = \mathbf{u}/\mathbf{u_c}$ and time $\tilde{\tau} = u_c t/L$. As surface tension influences the pressure, a natural choice for the characteristic pressure is the capillary pressure, such that $\tilde{p} = pL/\gamma$. Rewriting Equation (1) in terms of these non-dimensional variables with the pressure term pre-factor of unity leads to

$$\mathrm{We}\left(\frac{\partial \tilde{\mathbf{u}}}{\partial \tau} + \tilde{\mathbf{u}} \cdot \tilde{\nabla}\tilde{\mathbf{u}}\right) = -\tilde{\nabla}\tilde{p} + \mathrm{Ca}\tilde{\nabla}^2\tilde{\mathbf{u}} + \mathrm{Bo}\hat{\mathbf{z}}, \quad (2)$$

where three dimensionless parameters emerge. The Weber number $\mathrm{We} = \rho u_c^2 L/\gamma$ quantifies the relative importance of inertial and capillary forces. The capillary number $\mathrm{Ca} = \mu u_c/\gamma$ quantifies the relative importance of viscous and capillary forces and the Bond number

$$\mathrm{Bo} = \Delta\rho g L^2/\gamma \quad (3)$$

quantifies the relative importance of gravitational and capillary forces. Furthermore, if one or more of these dimensionless parameters is significantly smaller than the others, those terms in Equation (2) do not contribute significantly to the dominant dynamics; thus can be dropped, thereby simplifying the first-order analysis.

Perhaps, the best known dimensionless number in fluid mechanics is the Reynolds number

$$\mathrm{Re} = \rho u_c L/\mu, \quad (4)$$

which quantifies the relative balance of inertial and viscous effects. Quick inspection reveals that the Weber and capillary numbers can be related to the Reynolds number by $\mathrm{We}/\mathrm{Ca} = \mathrm{Re}$.

In some interfacial flows, the characteristic velocity is not imposed, but instead is established, based on a balance of underlying forces. For example, when capillary and inertial forces balance $\mathrm{We} = 1$, which occurs when $u_c = \sqrt{\gamma/\rho L}$. Substituting this characteristic velocity into Equation (4) yields the Ohnesorge number $\mathrm{Oh} = \mu/\sqrt{\rho\gamma L}$, a number that quantifies the relative importance of viscous and inertial effects in capillary flows. In this case, Equation (2) reduces to

$$\frac{\partial \tilde{\mathbf{u}}}{\partial \tau} + \tilde{\mathbf{u}} \cdot \tilde{\nabla}\tilde{\mathbf{u}} = -\tilde{\nabla}\tilde{p} + \mathrm{Oh}\tilde{\nabla}^2\tilde{\mathbf{u}} + \mathrm{Bo}\hat{\mathbf{z}}. \quad (5)$$

Here, the flow regime is determined by two dimensionless parameters: Oh and Bo.

The subsequent sections rely on the physical framework above to describe the interactions between a bubble and its surrounding biological environment. Throughout a bubble's life, the capillary forces can attract, stress, and disperse surrounding biomaterial. Similarly, this biomaterial can modify the capillary forces through, for example, producing or acting as a surfactant. When appropriate, our discussion will incorporate the concepts outlined in Fig. 3 and the dimensionless numbers presented in this section.

A bubble is born

Bubbles are ubiquitous across natural bodies of water, such as ponds, lakes, and oceans. These bubbles may be formed in any process that breaks the interface and entrains air into the water (Blanchard 1989), including rainfalls, snowfalls, and breaking waves. Here, we focus on breaking waves, as they are more common than rainfalls and snowfalls around the globe. Waves not only break at the shore (Fig. 1A), but also in the middle of the ocean when wind speeds are high enough to destabilize the surface waves [typically above 3 m/s (Blanchard 1963; Monahan 1971)]. The breaking

and the formation of whitecaps dissipate surface-wave energy and generate the mixing of gas and biomaterial via turbulence and bubble-entrainment (Melville 1996). Typically, whitecaps consist of a myriad of small bubbles rising to the surface. The size of such bubbles is estimated to range from micrometers to centimeters (Blanchard Woodcock 1957; Baldy and Bourguel 1987; Deane and Stokes 2002). Recent studies examined the spectrum of bubble-sizes (number of bubbles per meter cube per micrometer radius increment) generated early in the breaking of a wave and found two power-law scaling. The transition between these two scalings occurs at $R \approx 1$ mm in seawater and is related to the level of the rate of dissipation of turbulence. Small bubbles are subject to the stabilization of surface tension and scale as $R^{-3/2}$, whereas larger bubbles are subject to turbulence and shear, leading to frequent breakups that scale as $R^{-10/3}$ (Deane and Stokes 2002).

In artificial bodies of water, bubbles are created for aeration. Although other options for maintaining dissolved gas levels of oxygen and carbon dioxide (e.g., surface aeration) are available in small-scale bioreactors, direct injection of gas is essential when production scales are involved. Yet, there are some undesirable consequences; sparging has been shown in recent studies to have detrimental effects on cells near the region of bubble formation (Barbosa et al. 2003; Zhu et al. 2008; Liu et al. 2013). A widely used scalar parameter for quantifying cell damage in incompressible Newtonian fluids is the energy-dissipation rate ε (Liu et al. 2013). Ma et al. (2002) examined a variety of cells of industrial relevance and found that energy-dissipation rates of 10–100 W/cm^3 caused as many as 20% of the more sensitive cells to be damaged, specifically the mammalian cells which lack a protective cell wall. Such values are orders of magnitude higher than those achieved in a mixed tank (Wernersson and Trägårdh 1999), but are comparable with the energy dissipation of small bursting bubbles (Boulton-Stone and Blake 1993). Following the method of Cherry and Hulle (1992) we can estimate the energy dissipation as:

$$\varepsilon = \frac{1}{\pi r_{rim}^2}\left(\frac{2\gamma^3}{\rho h}\right)^{1/2}$$

with r_{rim} the radius of the retracting rim and h the bubble thickness (see Section "A bubble drains and dies"). For example, a water bubble with a radius of 1 mm and thickness of 10 μm yields an energy dissipation of 52 W/cm^3. While excessive hydrodynamic stresses are agreed to be one of the main causes for cell damage (Tramper et al. 1986; Garcia-Briones and Chalmers 1994), no model is able to relate the hydrodynamic forces to lethal and non-lethal cell effects (Hu et al. 2011).

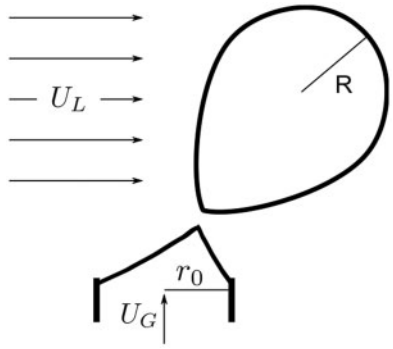

Fig. 4. Illustration of gas bubble with radius R being pinched-off at an orifice submerged in a liquid with cross-flow.

In sparged systems, the formation of a bubble occurs at an orifice via a complex process depending on the fluid's properties, the orifice's geometry, and the conditions of the surrounding flow (Kumar and Kuloor 1970; Miyahara and Hayashino 1995; Thoroddsen et al. 2007). However, in the simple case of slow injection of gas into a stagnant fluid we can approximate the bubble's radius by balancing the capillary $F_c = 2\pi r_0 \gamma$ and buoyancy forces $F_b = \frac{4}{3}\pi \Delta\rho g R^3$. By setting Bo = 1 based on the orifice's radius (r_0 in Fig. 4) the resulting radius of the bubble becomes $R = 1.14 r_0 \approx l_c$, in which $l_c = \sqrt{\gamma/\Delta\rho g}$ is the capillary length. The capillary length is the length scale at which gravitational and capillary effects are effectively balanced. For air bubbles surrounded by water, or alternatively water droplets surrounded by air, the capillary length is $l_c \approx 2$ mm.

As in stirred bioreactors, in most environments, the fluid surrounding bubbles is not stagnant but instead flows over the bubble-generating orifice (Fig. 4). This cross-flow exerts an additional force on the bubble leading to a shift of its detachment from being buoyancy-dominated to shear dominated. This shearing force will encourage early detachment from the orifice, resulting in smaller bubbles being produced more frequently than in the case of stagnant fluid. Not only does a cross-flow reduce the size of bubbles exiting from a single orifice, but it also reduces the frequency of coalescence among adjacent bubbles in closely spaced orifices like those commonly found on spargers. Ultimately, a more uniform and predictable distribution of bubble sizes can be produced (Maier 1927; Sullivan et al. 1964).

A bubble's journey upwards

The purpose of sparging and other types of aeration techniques is to control the level of a dissolved gas in a life-supporting fluid medium. As a bubble rises, mass transfer occurs at its interface. The mass transfer rate j_b is driven by the difference in gas concentration between the inner and outer regions of the bubble, with $j_b = 4\pi R^2 k_L(c_b - c_\infty)$, where c_b and c_∞ are the concentrations of gas in the bubble and surrounding fluid, and k_L is the mean mass transfer coefficient (Gong et al. 2007). The concentration of dissolvable gas in the bubble is related to the partial pressure of the gas inside p_b through Henry's law:

$$p_b = Hc_b$$

Here, the Henry constant H has units of $\frac{L \cdot atm}{mg}$ and is experimentally determined for specified combinations of liquid and gas at a fixed temperature. The mass change inside the bubble $j_b = \frac{d}{dt}\left(\frac{4}{3}\pi R^3 \rho_g\right)$ can be simplified to $j_b \approx 4\pi R^2 \rho_G \frac{dR}{dt}$ as contribution from the second term containing $\frac{d\rho_G}{dt}$ was shown experimentally to be <2% and can be neglected (Takemura and Yabe 1999). Equating these relations and utilizing the ideal gas law yields an expression for the rate at which a bubble shrinks as it dissolves:

$$\frac{dR}{dt} = \frac{p_b - p_\infty}{p_b}\frac{\Re T k_L}{H} \tag{6}$$

Here, p_∞ is the equivalent pressure of the dissolved gas in the liquid, $\Re$ is the specific gas constant, and T is the absolute temperature.

An interesting result of Equation (6) is that a bubble will be driven to dissolve even when the surrounding fluid is saturated due to the capillary pressure increase. Although small bubbles with high internal pressure favor dissolution, observations have shown that bubbles with $R < 60\,\mu$m may persist indefinitely in the ocean (Mulhearn 1981). This phenomenon has been attributed to the bubbles being coated with natural surfactants, thereby inhibiting mass transfer (Czerski et al. 2011). The primary source of these surfactants appears to be phytoplankton exudates (Žutić et al. 1981; Wurl et al. 2011).

The rise of a bubble through its surroundings is driven by the buoyancy force F_b (Section "Origin and relevance of capillarity") and is resisted by the fluid leading to an interfacial stress (τ in Fig. 3). For example, a bubble dominated by viscosity and surface tension, specifically small Re and Bo numbers, rising in an ideally clean fluid will be approximately spherical and possess a mobile interface. The fluid

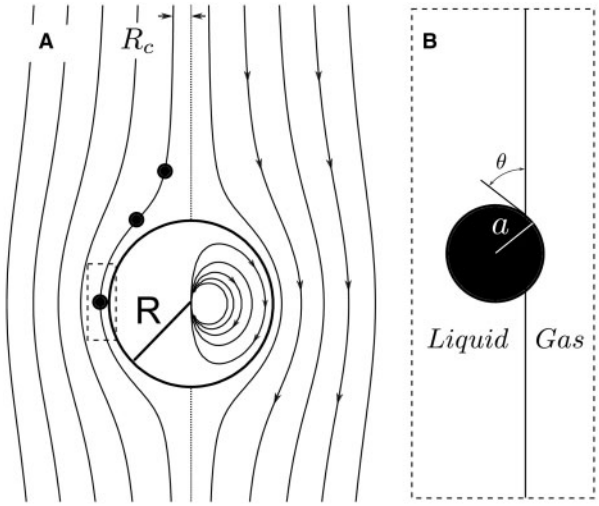

Fig. 5. The rise of a spherical bubble in a fluid. (A) Illustrates on the right half the rise of a bubble in a clean environment. The left half illustrates a rigid interface with a particle contacting and adhering. (B) Close-up view of boxed particle in A that has formed a three-phase contact angle.

inside the bubble will move toroidally while the surrounding fluid will diverge and re-convergent behind the bubble to allow its passage as shown in Fig. 5. In this case, the terminal rise velocity is given by the Hadamard–Rybczynski equation (Hadamard 1911; Rybczynski 1911):

$$\frac{u_t}{u_c} = \frac{2}{9}\mathrm{Re}\left(1 - \frac{\rho_g}{\rho_l}\right)\left(\frac{1 + \frac{\mu_l}{\mu_g}}{1 + \frac{2}{3}\frac{\mu_l}{\mu_g}}\right) \tag{7}$$

wherein the characteristic velocity $u_c = \sqrt{gR}$ is now given in terms of gravity, the driving force behind the bubble's rise. For an air bubble in water Equation (7) can be simplified to $\frac{u_t}{u_c} = \frac{1}{3}\mathrm{Re}$ owing to the large density and viscosity differences. However, as the bubble rises, the liquid encountered is rarely pure and instead filled with suspended material, such as particulates and microorganisms. When such surfactants are present in the fluid, they end up being scavenged by the rising bubble. Such scavenging leads to local changes of surface tension on the rising bubble's surface. The Marangoni stresses induced by these gradients resist the motion of the interface towards the back of the bubble, thus rendering the bubble's surface nearly immobile. The surface of the bubble behaves as if it was rigid.

In such cases, $\mu_g \gg \mu_l$ and Equation (7) limits to the familiar Stoke's law $\frac{u_t}{u_c} = \frac{2}{9}\mathrm{Re}$ (Clift et al. 1978). Thus, smaller bubbles with surface contamination dwell in the water ~50% longer than surfactant free bubbles.

As a bubble approaches a suspended particle, the particle will either pass around, or collide with, the bubble's surface (Fig. 5A). In the event of a particle–bubble collision it is possible for the particle not to attach permanently to the free surface (Miettinen et al. 2010). For attachment to occur, the liquid between the particle and the thin bubble film must completely drain to allow for a three-phase contact line to develop (Fig. 5B) (Verrelli et al. 2011). The time required for this process to occur is known as the induction time and must be less than the time required for the particle to simply "slide" around and off the back of the bubble. The induction time is predominantly influenced by surface chemistry, although few experimental studies have thoroughly examined this phenomenon as it naturally occurs (Verrelli et al. 2011).

In the event of attachment upon particle–bubble collision (Fig. 5A) the concentration of particles at the surface of the rising bubble will become enriched when compared with that of the fluid bulk (Blanchard and Syzdek 1970, 1972, 1982; Wallace et al. 1972; Burger and Bennett 1985). This effect can be quantified with the collision efficiency as defined by the ratio of particles attached to the bubble at the surface to the total number of particles in the volume swept out by the bubble during its rise

$$E_{col} = \frac{\#\text{ of particles attached}}{\#\text{ of particles in volume swept}} \qquad (8)$$

Numerous factors can influence the collision efficiency, including particle–bubble size ratio, the mobility of the bubble's surface, and the hydrophobicity or hydrophilicity of the particle (Yoon and Luttrell 1989; Dai et al. 2000). Perhaps one of the simplest models of bubble–particle collision assumes that the particle's inertia can be neglected owing to their small size, thus allowing them to follow the flow streamlines, as illustrated in Fig. 5A, and enabling estimation of the number of collisions. This model assumes that the Reynolds number of the bubble is sufficiently high, as opposed to Stoke's law case, to allow for the neglect of viscous or rotational effects, and that the bubble's surface is fully mobile (Sutherland 1948). This particular model applies when the Reynolds number is between 80 and 500. Given such assumptions, a distance from the bubble's center-line R_c under which all particles will collide and attach can be derived $R_c = \sqrt{3aR}$ (Fig. 5A). The collision efficiency E_{col} can then be computed via Equation (8). By taking the ratio of the collision tube's area $3\pi aR$ to the projected area of the bubble πR^2, the collision efficiency simplifies to $E_{col} = 3a/R$.

Despite the numerous assumptions built into the model above, the Sutherland collision efficiency has provided the foundation for many recent collision models (e.g., Dai et al. 2000). However, numerous factors can lead to the breakdown of the most fundamental assumptions. In particular, as discussed above, the mobility of the surface needs revision. In fact, an immobile surface always results in a lower collision efficiency owing to the fluid streamlines being forced away from the interface (Schulze 1992). More recent models of bubble–particle collision relaxed some of Sutherland's (1948) assumptions and were used to explain the enrichment of cells and bacteria attached to rising bubbles (Weber et al. 1983; Meier et al. 1999).

A bubble drains and dies

When a gas bubble rises to the surface of a liquid, it deforms the air–liquid interface. Toba (1959) and Princen (1963) independently reasoned that, at the fluid's interface, these bubbles reach an equilibrium shape that depends on the relative effects of gravity and surface tension, as quantified by the Bond number Equation (3). The bubble in Fig. 2C illustrates a schematic of one of these equilibrium shapes. The thin film separating the gas in the bubble from the gas outside the bubble is assumed to be of uniform thickness. Its overall shape is close to spherical, depending on the size of the bubble. This shape minimizes surface energy.

Once the bubble reaches its equilibrium surface shape, the liquid in its film drains back into the surrounding pool by a combination of gravitational draining and capillary suction; the relative strength of these draining mechanisms again depends on the Bond number or the size of the bubble. When small amounts of surfactant are present—as is the case for fluids containing biomass—the surfactant on the bubble's cap drains along with the liquid, leading to a gradient in surface tension (Stein 1993). The effect of this gradient is a Marangoni stress that counteracts the drainage (Fig. 3) and increases the persistence time of the bubble at the surface (Mysels et al. 1959). Regardless of the draining mechanism, the film eventually becomes thin enough for molecular forces to become destabilizing and cause rupture.

Indeed, the surface area of a bubble's thin shell is significantly greater than that of a spherical droplet of an identical volume of liquid. Thus, thin film caps are only local rather than global surface energy minima. In other words, small perturbations to a bubble's film surface area are attenuated. Yet,

sufficiently large geometrical perturbation can lead to the development of a hole that will grow, resulting in the death or burst of the bubble. In particular, an initial hole can grow.

While the film remains thick enough, the initial hole can be induced by an external force resulting from direct contact with solid objects or the deposition of dust particles. As thinning progresses, spontaneous popping can eventually occur when the film's thickness becomes on the order of tens of nanometers, a scale at which Van der Waals forces are no longer negligible (Vrij 1966). However, such thickness is much smaller than that commonly observed prior to the burst of water bubbles with small surfactant concentrations, which is on the order of 0.1–10 μm. Once formed, the hole will grow if its size is larger than twice the thickness of the bubble film (Taylor and Michael 1973). Indeed, although it is unclear what initiates the rupture in these instances, experiments have demonstrated that the thickness of bubbles at burst decreases with decreasing surface tension and increases with size of the bubble, specifically $h \propto R^2$ (e.g., Modini et al. 2013 and references therein).

When a hole nucleates, its growth—or more precisely the retraction of the film—is driven by capillary forces due to the decrease in surface energy (Fig. 6). The dynamics of this retraction have been investigated for over a century. Dupré is credited for initially recognizing that when a hole nucleates in a thin sheet of liquid, the film around the hole collects into a growing rim while the rest of the film remains essentially still (Dupré 1867). By assuming that all of the surface energy released by the decrease in surface area is converted into the kinetic energy of the retracting rim, Dupré calculated that the film would retract at a constant velocity. These results were echoed shortly later by Rayleigh who carried out some of the earliest high-speed visualization (Rayleigh 1878), then again by De Vries (1958). Yet, more precise experiments by Ranz (1958) suggested that Dupré's calculation overestimated the velocity of retraction, motivating Culick (1960) to recognize that half of the surface energy is dissipated in the rim. Meanwhile, Taylor independently arrived at the same theoretical velocity while investigating retracting sheets (Taylor 1959).

Figure 6 illustrates the interaction of the retracting film with cells or other biologically relevant material. The relevant acceleration and the dissipation of energy experienced by these cells can be calculated by considering a force balance on the boundary of the retracting rim (dashed oval in Fig. 6). Assuming that the sheet is flat with width w, the capillary force F pulling on the rim is $2\gamma w$, where the factor of 2 is the result of there being an interface both above and below the film. This force is balanced by the change in momentum of the rim with respect to time. For a given velocity of retraction V, the mass of the rim increases at a rate of ρwhV, where ρ is the fluid's density and h is the film's thickness. Therefore, we arrive at constant retraction velocity $V = \sqrt{2\gamma/\rho h}$. The retraction velocity is identical for a spherical thin film geometry, as illustrated by Pandit and Davidson (1990) using both experiments and calculations. For a 5-μm sheet of water, such retraction velocity is over 5 m/s. If particles were accelerated to this velocity over the distance of a 10-μm rim, the acceleration would be over 2×10^6 m/s^2, or 200,000 g. While this intense acceleration might be fatal for certain cells (Chalmers and Bavarian 1991), recent research suggests that many microorganisms can still thrive under such conditions (Deguchi et al. 2011).

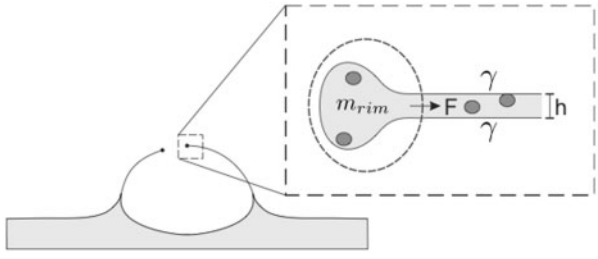

Fig. 6. As a hole opens in the rupturing bubble, the liquid film is collected into a growing rim. Capillary driving forces balance inertial forces in such a way that the velocity of the retracting rim is nearly constant. As is seen in the boxed section, there are two liquid-gas interfaces (indicated by γ on the top and bottom).

A bubble's legacy lives on

Even following its death, a bubble can still impact its surroundings. Specifically, the rupture of the bubble can generate and disperse particulate or pathogen-filled droplets (Fig. 7) as well as create numerous

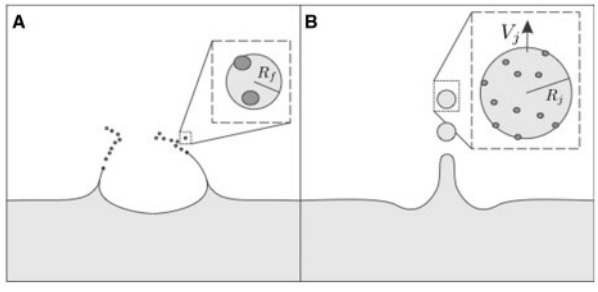

Fig. 7. (A) Film drops and (B) jet drops can be a vector for biomaterial.

smaller bubbles that themselves can rise to the surface and rupture. These droplets can persist in the air due to their small size, and have been linked to the transfer of pathogens and disease (Parker et al. 1983; Embil et al. 1997; Falkinham 2003; Bourouiba and Bush 2012).

It was perhaps first Plateau (1873), upon reviewing the results of Dupré (1867), who recognized that the retracting rim of a bubble could become unstable and lead to the generation of hundreds of drops. These drops are referred to as film drops as they originate from the bubble film destabilization as illustrated in Fig. 7A. Attention has been given to the number and size of these film drops (e.g., Mason 1954; Day 1964; Afeti and Resch 1990; Spiel 1998) including when the film drops contained bacteria (Blanchard and Syzdek 1982). Numerous analytical and empirical relations have been proposed (e.g., Lewis and Schwartz 2004). For example, Mason (1954) reported 100–200 film droplets from bubbles of 0.5–3 mm diameter, whereas the number of film droplets for a bubble <0.5 mm quickly decays (Lewis and Schwartz 2004). Perhaps some of the most convincing relations were proposed by Lhuissier and Villermaux (2011) who reasoned that the number N and size R_f of film drops should scale as $N \sim (R/l_c)^2 (R/h)^{7/8}$ and $R_f \sim R^{3/8} h^{5/8}$. Here R is the radius of the bubble, l_c is the capillary length, and h is the thickness of the bubble at rupture, assumed to range from 10 to 1000 μm. Surface tension and surfactants play a role in setting both the capillary length, as well as the thickness when the bubble bursts (Modini et al. 2013).

After the film has completed retracted, capillary forces rapidly close the remaining air cavity, often leading to the formation of another family of drops. Indeed, a jet reminiscent of the classical Worthington jet (Worthington and Cole 1897) rises upward and can become unstable; hence also producing droplets (Fig. 7B). Such droplets are referred to as jet drops and their size and composition could be different from that of film drops (Woodcock et al. 1953; MacIntyre 1972; Blanchard 1989).

Experimental results demonstrate that the size of these jet drops R_j is ~5–20% of the original bubble's radius R. For example, a so-called 10% rule was proposed by Kientzler et al. (1954) when observing up to five jet drops from bubbles of diameters ranging from 0.2 to 1.8 mm. Subsequent experiments developed more precise empirical relations between the sizes of jet droplets, their speeds and the original bubbles' sizes (e.g., Blanchard 1989; Spiel 1994, 1998; Lewis and Schwartz 2004). For a water bubble with a radius >3 mm (Bo > 1), capillary forces are not able to overcome the weight of the jet, and jet drops are seldom formed. Smaller bubbles—typically of <0.5 mm diameter—are observed to have more; yet at sufficiently small scales, viscous forces would eventually inhibit jet drops from forming. Indeed recent experiments using ultrafast X-ray imaging have suggested that jets stop being produced at an Ohnesorge value of Oh ≈ 0.052, which would correspond to a water bubble of 4 μm in radius (Lee et al. 2011). Nevertheless, it has been argued that few jet drops at this scale would actually be produced on the ocean's surface, and even fewer would be dispersed into the atmosphere (Lewis and Schwartz 2004). In the event that a 5-μm bubble were to pop at the surface, the maximum height reached by its daughter jet drops would be only 400 μm (Blanchard 1989), thus limiting their ability to escape the boundary layer created by wind moving across the ocean surface.

The potential for a single bubble to generate both film drops and jet drops has long been appreciated (Knelman et al. 1954). Yet, the relative number and sizes of these droplets tend to be quite different. As suggested by the scaling relations, larger bubbles (diameter >3 mm) tend to be dominated by film drops, whereas smaller bubbles tend to be dominated by jet drops. Additionally, for a given bubble, film drops tend to be smaller than jet drops.

Finally, in addition to creating droplets, a bubble can also create smaller, daughter bubbles as it ruptures (e.g., MacIntyre 1972; Herman and Mesler 1987; Bird et al. 2010). These daughter bubbles can follow a similar life to their parent, rising, scavenging, and eventually rupturing; yet they carry out this progression while being at a smaller size. Therefore, a bubble that may have been too large to create jet drops may generate numerous bubbles that each will propel numerous jet drops (and their contents) into the atmosphere.

Concluding remarks

From the open ocean to the shores; from indoor pools to bioreactors, bubbles are ubiquitous in bodies of water. As we see in this review, their role is multifaceted. Whether their role is desirable (e.g., for aeration or for transport of biomaterial) or harmful (e.g., outbreaks of disease along shores or indoors, or damage of cell cultures) bubbles deeply connect physics to biology through subtle interfacial fluid dynamics. Despite a relatively old identification of bubbles as physical and biological mixers and as creators of droplets, a range of fundamental

questions pertaining to their interaction with the microorganismal world remain widely open. For example, the response of cells to subcellular level hydrodynamic forces is not understood; as performance is increased, non-lethal, negative effects may emerge (Hu et al. 2011). At the air–ocean interface, it is still unclear whether the stress of bubble rupture damages certain organisms as observed in bioreactors, thereby emitting certain types or sizes selectively or more readily than others. Indoor, the subtle role of the life and death of bubbles at the interface of contaminated water (e.g., in hospitals, therapeutic, or care facilities) in selecting certain pathogens for new routes of disease transmission remain unclear. In this brief review, we hope to have guided the reader through the rich life of a bubble and highlighted the many areas in which fluid dynamics can be of help in understanding bubbles; interactions with the world of the small.

Acknowledgments

We thank the divisions within the Society of Integrative and Comparative Biology, including the Division of Comparative Biomechanics, the Division of Vertebrate Morphology, the Division of Invertebrate Zoology, and the American Microscopy Society for their support.

Funding

NSF (1347346 to L.B.); NSF CAREER award (1351466 to J.C.B.).

References

Afeti GM, Resch FJ. 1990. Distribution of the liquid aerosol produced from bursting bubbles in sea and distilled water. Tellus B 42B:378–84.

Angelini TE, Roper M, Kolter R, Weitz DA, Brenner MP. 2009. Bacillus subtilis spreads by surfing on waves of surfactant. Proc Natl Acad Sci 106:18109–13.

Baldy S, Bourguel M. 1987. Bubble between the wave trough and wave crest levels. J Geophys Res 92:2919–29.

Barbosa MJ, Albrecht M, Wijffels RH. 2003. Hydrodynamic stress and lethal events in sparged microalgae cultures. Biotechnol Bioeng 83:112–20.

Bauer H, Fuerhacker M, Zibuschka F, Schmid H, Puxbaum H. 2002. Bacteria and fungi in aerosols generated by two different types of wastewater treatment plants. Water Res 36:3965–70.

Berg JC, Boudart M, Acrivos A. 1966. Natural convection in pools of evaporating liquids. J Fluid Mech 24:721–35.

Bhaga D, Weber ME. 1981. Bubbles in viscous liquids: shapes, wakes and velocities. J Fluid Mech 105:61–85.

Bird JC, de Ruiter R, Courbin L, Stone HA. 2010. Daughter bubble cascades produced by folding of ruptured thin films. Nature 465:759–62.

Blanchard DC. 1963. The electrification of the atmosphere by particles from bubbles in the sea. Progr Oceanogr 1:73–202.

Blanchard DC. 1989. The size and height to which jet drops are ejected from bursting bubbles in seawater. J Geophys Res 94:999–11002.

Blanchard DC, Syzdek L. 1970. Mechanism for the water-to-air transfer and concentration of bacteria. Science 170:626–8.

Blanchard DC, Syzdek L. 1972. Concentration of bacteria in jet drops from bursting bubbles. J Geophys Res 77:5087–99.

Blanchard DC, Syzdek L. 1982. Water-to-air transfer and enrichment of bacteria in drops from bursting bubbles. Applied Environ Microbiol 43:1001–5.

Blanchard DC, Woodcock AH. 1957. Bubble formation and modification in the sea and its meteorological significance. Tellus B 9:145–58.

Boulton-Stone J, Blake J. 1993. Gas bubbles bursting at a free surface. J Fluid Mech.

Bourouiba L, Bush JWM. 2012. Drops and bubbles in the environment. In: Handbook of environmental fluid dynamics, Volume one: overview and fundamentals. Boca Raton (FL): CRC Press, Taylor & Francis Group. p. 427–40.

Boyce SG. 1951. Source of atmospheric salts. Science 113:620–1.

Burger S, Bennett J. 1985. Droplet enrichment factors of pigmented and nonpigmented Serratia marcescens: possible selective function for prodigiosin. Appl Environ Microbiol 50:487–90.

Chalmers JJ, Bavarian F. 1991. Microscopic visualization of insect cell-bubble interactions. II: The bubble film and bubble rupture. Biotechnol Progr 7:151–8.

Cherry R, Hulle C. 1992. Cell death in the thin films of bursting bubbles. Biotechnol Progr 8:11–8.

Chisti Y. 2000. Animal-cell damage in sparged bioreactors. Trends Biotechnol 18:420–32.

Clift R, Grace JR, Weber ME. 1978. Bubbles, drops, and particles. New York (NY): Academic Press, Inc.

Culick F. 1960. Comments on a ruptured soap film. J Appl Phys 31:1128–9.

Czerski H, Twardowski M, Zhang X, Vagle S. 2011. Resolving size distributions of bubbles with radii less than 30 μm with optical and acoustical methods. J Geophys Res 116:C00H11.

Dai Z, Fornasiero D, Ralston J. 2000. Particle-bubble collision models–a review. Adv Colloid Interfac 85:231–56.

Day JA. 1964. Production of droplets and salt nuclei by the bursting of air-bubble films. Q J Roy Meteor Soc 90:72–8.

Deane GB, Stokes MD. 2002. Scale dependence of bubble creation mechanisms in breaking waves. Nature 418:839–44.

Deguchi S, Shimoshigea H, Tsudomea M, Mukaia M-a, Corkery RW, Ito S, Horikoshia K. 2011. Microbial growth at hyperaccelerations up to 403,627 x g. Proc Natl Acad Sci USA 108:7997–8002.

Dupré A. 1867. Sixieme memoire sur la theorie mécanique de la chaleur (in French). Ann Chim Phys 11:194–220.

Embil J, Warren P, Yakrus M, Stark R, Corne S, Forrest D, Hershfield E. 1997. Pulmonary illness associated with exposure to mycobacterium-avium complex in hot tub water* hypersensitivity pneumonitis or infection? Chest 111:813–6.

Falkinham III, JO. 2003. Mycobacterial aerosols and respiratory disease. Emerg Infect Dis 9:763–7.
Garcia-Briones MA, Chalmers JJ. 1994. Flow parameters associated with hydrodynamic cell injury. Biotechnol Bioeng 44:1089–98.
Gong X, Takagi S, Huang H, Matsumoto Y. 2007. A numerical study of mass transfer of ozone dissolution in bubble plumes with an Euler–Lagrange method. Chem Eng Sci 62:1081–93.
Hadamard J. 1911. Mouvement permanent lent d'une sphere liquide et visqueuse dans un liquide visqueux (in French). CR Acad Sci 152:1735–8.
Herman J, Mesler R. 1987. Bubble entrainment from bursting bubbles. J Colloid Interfac 117:565–9.
Hosoi AE, Bush JWM. 2001. Evaporative instabilities in climbing films. J Fluid Mech 442:217–39.
Hu W, Berdugo C, Chalmers JJ. 2011. The potential of hydrodynamic damage to animal cells of industrial relevance: current understanding. Cytotechnology 63:445–60.
Jacobs W. 1937. Preliminary report on a study of atmospheric chlorides. Monthly Weather Rev 65:147–51.
Kientzler C, Arons AB, Blanchard DC, Woodcock AH. 1954. Photographic investigation of the projection of droplets by bubbles bursting at a water surface1. Tellus B 6:1–7.
Knelman F, Dombrowski N, Newitt D. 1954. Mechanism of the bursting of bubbles. Nature 4397:261.
Kumar R, Kuloor NR. 1970. The formation of bubbles and drops. Adv Chem Eng 8:255–368.
Laitinen S, Kangas J, Kotimaa M, Liesivuori J, Martikainen PJ, Nevalainen A, Sarantila R, Husman K. 1994. Workers' exposure to airborne bacteria and endotoxins at industrial wastewater treatment plants. Am Ind Hyg Assoc J 55:1055–60.
Lee JS, Weon BM, Park SJ, Je JH, Fezzaa K, Lee W-H. 2011. Size limits the formation of liquid jets during bubble bursting. Nat Commun 2:367.
Lewis R, Schwartz E. 2004. Sea salt aerosol production: mechanisms, methods, measurements and models—a critical review. Washington (DC): American Geophysical Union.
Lhuissier H, Villermaux E. 2011. Bursting bubble aerosols. J Fluid Mech 696:5–44.
Liu Y, Li F, Hu W, Wiltberger K, Ryll T. 2013. Effects of bubbleliquid two-phase turbulent hydrodynamics on cell damage in sparged bioreactor. Biotechnol Progr 30:48–58.
Ma N, Koelling KW, Chalmers JJ. 2002. Fabrication and use of a transient contractional flow device to quantify the sensitivity of mammalian and insect cells to hydrodynamic forces. Biotechnol Bioeng 80:428–37.
MacIntyre F. 1972. Flow patterns in breaking bubbles. J Geophys Res 77:5211–28.
Magnaudet J, Eames I. 2000. The motion of high-Reynolds-number bubbles in inhomogeneous flows. Annu Rev Fluid Mech. 659–708.
Maier CG. 1927. The ferric sulphate-sulphuric acid process: with a chapter on producing small bubbles of gas in liquids by submerged orifices. Washington: United States Government Printing Office.
Marangoni C. 1865. On the expansion of a drop of liquid floating on the surface of another liquid. Pavia, Italy: Tipographia dei fratelli Fusi.
Mason BJ. 1954. Bursting of air bubbles at the surface of sea water. Nature 174:470–1.
Meier SJ, Hatton T, Wang DI. 1999. Cell death from bursting bubbles: role of cell attachment to rising bubbles in sparged reactors. Biotechnol Bioeng 62:468–78.
Melville WK. 1996. The role of surface-wave breaking in air-sea interaction. Annu Rev Fluid Mech 28:279–321.
Miettinen T, Ralston J, Fornasiero D. 2010. The limits of fine particle flotation. Minerals Engineering, 23:420–37.
Miyahara T, Hayashino T. 1995. Size of bubbles generated from perforated plates in non-Newtonian liquids. J Chem Eng Jpn 28:596–600.
Modini RL, Russell LM, Deane GB, Stokes MD. 2013. Effect of soluble surfactant on bubble persistence and bubble-produced aerosol particles. J Geophys Res-Atmos 118: 1388–400.
Monahan E. 1971. Oceanic whitecaps. J Phys Oceanogr 1:139–44.
Mulhearn PJ. 1981. Distribution of microbubbles in coastal waters. J Geophys Res 86:6429.
Murhammer DW, Goochee CF. 1990. Sparged animal cell bioreactors: mechanism of cell damage and Pluronic F-68 protection. Biotechnol Progr 6:391–7.
Mysels KJ, Shinoda K, Frankel S. 1959. Soap films: studies of their thinning and a bibliography. Oxford: Pergamon Press Ltd.
Pandit A, Davidson J. 1990. Hydrodynamics of the rupture of thin liquid films. J Fluid Mech 212:11–24.
Parker BC, Ford MA, Gruft H, Falkinham JO 3rd. 1983. Epidemiology of infection by nontuberculous mycobacteria. IV. Preferential aerosolization of Mycobacterium intracellulare from natural waters. Am Rev Respir Dis 128:652–6.
Plateau J. 1873. Experimental and theoretical statics of liquids subject to molecular forces only. Paris: Gauthier-Villars.
Princen H, 1963. Shape of a fluid drop at a liquid-liquid interface. J Colloid Sci 18:178–95.
Ranz WE. 1958. Some experiments on the dynamics of liquid films. J Appl Phys 30:1950–5.
Rayleigh L. 1878. On the instability of jets. P Lond Math Soc 10:4–13.
Rybczynski W. 1911. On the translatory motion of a fluid sphere in a viscous medium. Bull Acad Sci Cracow Ser A 40:40–6.
Schulze HJ. 1992. Probability of particle attachment on gas bubbles by sliding. Adv Colloid Interfac 40:283–305.
Scriven LE, Sternling CV. 1960. The Marangoni effects. Nature 187:186–8.
Spiel DE. 1994. The sizes of the jet drops produced by air bubbles bursting on sea- and fresh-water surfaces. Tellus B 46:325–38.
Spiel DE. 1998. On the births of film drops from bubbles bursting on seawater surfaces. J Geophys Res 103:24907–18.
Stein HN. 1993. The drainage of free liquid films. Colloid Surface A 79:71–80.
Stuhlman O. 1932. The mechanics of effervescence. Physics 2:457.
Sullivan SL, Hardy BW, Holland CD. 1964. Formation of air bubbles at orifices submerged beneath liquids. AIChE J 10:848–54.
Sutherland K. 1948. Physical chemistry of flotation. XI. Kinetics of the flotation process. J Phys Chem 52:394–425.

Takemura F, Yabe A. 1999. Rising speed and dissolution rate of a carbon dioxide bubble in slightly contaminated water. J Fluid Mech 378:319–34.

Taylor G. 1959. The dynamics of thin sheets of fluid. III. Disintegration of fluid sheets. P Roy Soc Lond 253:313–21.

Taylor GI, Michael DH. 1973. On making holes in a sheet of fluid. J Fluid Mech 58:625–39.

Thoroddsen ST, Etoh TG, Takehara K. 2007. Experiments on bubble pinch-off. Phys Fluids 19:042101.

Toba Y. 1959. Drop production by bursting of air bubbles on the sea surface (II) Theoretical study of the shape of floating bubbles. J Oceanogr Soc Jap 15:121–30.

Tramper J, Williams JB, Joustra D, Vlak JM. 1986. Shear sensitivity of insect cells in suspension. Enzyme Microb Tech 8:33–6.

Verrelli DI, Koh PTL, Nguyen AV. 2011. Particle–bubble interaction and attachment in flotation. Chem Eng Sci 66:5910–21.

De Vries AJ. 1958. Foam stability: Part IV. Kinetics and activation energy of film rupture. Recueil des travaux chimiques des Pays-Bas 77:383–99.

Vrij A. 1966. Possible mechanism for the spontaneous rupture of thin, free liquid films. Discuss Faraday Soc 42:23–33.

Wallace G, Loeb G, Wilson D. 1972. On the flotation of particulates in sea water by rising bubbles. J Geophys Res 77:5293–301.

Weber M, Blanchard D, Syzdek L. 1983. The mechanism of scavenging of waterborne bacteria by a rising bubble. Limnol Oceanogr 28:101–5.

Wernersson ES, Trägårdh C. 1999. Scale-up of Rushton turbine-agitated tanks. Chem Eng Sci 54:4245–56.

Woodcock AH. 1948. Note concerning human respiratory irritation associated with high concentrations of plankton and mass mortality of marine organisms. J Mar Res 7:56–62.

Woodcock AH, Kientzler CF, Arons AB, Blanchard DC. 1953. Giant condensation nuclei from bursting bubbles. Nature 172:1144–5.

Worthington AM, Cole RS. 1897. Impact with a liquid surface, studied by the aid of instantaneous photography. Philos T Roy Soc A 189:137–48.

Wurl O, Wurl E, Miller L, Johnson K, Vagle S. 2011. Formation and global distribution of sea-surface microlayers. Biogeosciences 8:121–35.

Yoon RH, Luttrell GH. 1989. The effect of bubble size on fine particle flotation. Miner Process Extr Metall Rev 5:101–22.

Zhu Y, Cuenca JV, Zhou W, Varma A. 2008. NS0 cell damage by high gas velocity sparging in protein-free and cholesterol-free cultures. Biotechnol Bioeng 101:751–60.

Žutić V, Ćosović B, Marčenko E, Bihari N, Kršinić F. 1981. Surfactant production by marine phytoplankton. Mar Chem 10:505–20.